Master Thesis

Complete Wetting in the Potts Model

Daliah Maurer

2012

Supervisor

Prof. Uwe-Jens Wiese

Institute for Theoretical Physics, University of Bern

Abstract

The topic of this thesis is the three-dimensional Potts model with spins in $\mathbb{Z}(3)$. The model is simulated with the Swendsen-Wang cluster algorithm using periodic boundary conditions. In this way and because of the first order phase transition of this model at the critical point complete wetting can be observed and analyzed. In order to get the interface tension σ_{cd}, which describes the free energy per area of an interface between a section of ordered an disordered phase, two different quantities are measured. The final result of the interface tension is $\sigma_{cd} = 0.0015(2)$ resp. $\sigma_{cd} = 0.0016(2)$.

Contents

1 Introduction **5**

2 The Potts model **6**

2.1 Preface . . . 6

2.2 Symmetries . . . 9

2.3 Phases and phase transition . . . 9

2.4 Wetting . . . 9

2.5 The interface tension and the spectrum of the transfer matrix . . . 11

3 Numerical simulation **14**

3.1 The Monte Carlo method . . . 14

3.2 The Swendsen-Wang cluster algorithm . . . 15

3.2.1 Description of the simulation . . . 15

3.2.2 Ergodicity . . . 15

3.2.3 Normalization . . . 15

3.2.4 Detailed balance . . . 16

3.3 Estimators . . . 17

3.4 Data analysis . . . 18

3.4.1 How to fit the Monte Carlo Data . . . 18

3.4.2 Rough estimator of $E_{1,2}$ and E_3 . . . 19

4 Numerical results **21**

4.1 Comparison of the analytical solution and the simulation results . . . 21

4.2 Comparison with independent results . . . 22

4.3 Comparison of the improved and unimproved estimators . . . 23

4.4 The energies measured at different κ-values . . . 24

4.5 The interface tension σ_{cd} . . . 26

5 Conclusions **29**

5.1 Summary . . . 29

5.2 Comparison of the obtained σ_{cd} with results from the literature 29
5.3 Improvements 30

6 Acknowledgements **31**

A Correlation functions analytically **32**

B The trace of transfer matrix products **35**

List of Figures

2.1 Illustration of the spins and the spin configurations 6
2.2 How to imagine the transfer matrix 8
2.3 Complete and incomplete wetting 10
2.4 Configuration of a $21 \times 21 \times 250$ lattice with $\kappa = 0.55025$ 11
2.5 Graphical description of the transfer matrix elements 12

3.1 Comparision of the two ways to estimate the plateaus 20
3.2 $\mathsf{corr}_1(x_3)$ of a $17 \times 17 \times 250$ lattice at $\kappa = 0.54875$ 20

4.1 Comparison of exact and simulated results of the estimators 22
4.2 Plot of the estimator of $\langle \widetilde{\mathcal{O}_1}^*(0)\widetilde{\mathcal{O}_1}(x_3)\rangle$ 23
4.3 Plot of the energy values of a $21 \times 21 \times 250$ lattice 24
4.4 Plot of the estimator of $\langle \widetilde{\mathcal{O}_1}^*(0)\widetilde{\mathcal{O}_1}(x_3)\rangle$ on a $21 \times 21 \times 250$ lattice 25
4.5 Estimator of $\langle \widetilde{\mathcal{O}_1}^*(0)\widetilde{\mathcal{O}_1}(x_3)\rangle$ of two lattices with $A = 20^2$ and $\kappa = 0.5502$ . . . 26
4.6 The energy values as a function of the lattice cross-section A are plotted. 26
4.7 Illustration of the κ interval where the phase transition occurs 27

List of Tables

3.1 List of probabilities to activate bonds 15

4.1 Comparison of improved and unimproved estimators 23

Chapter 1

Introduction

In condensed matter physics different kind of phase transitions are explored. A simple example of a phase transition is boiling water in a closed box. There molecules in the liquid phase of water transform to the gaseous phase and vice versa. In this box an interface separating the liquid phase from the gaseous phase is built naturally. The free energy per area of such an interface is denoted as the „interface tension“. There exist models with phase transitions between more than two different phases. In quantum field theory the gluons can be described with such models as for example the SU(3) Yang-Mills theory at high temperatures.

In this work the three-dimensional Potts model with spins in $\mathbb{Z}(3)$ is simulated using the Swendsen-Wang cluster algorithm. „The Potts model is an important testing ground for the different methods and approaches in the study of the critical point theory.“, says [10]. According to [2] previous numerical studies of interface tensions were done by keeping different parts of the lattice at different temperatures or by applying an external field. Here interfaces are generated by the particular geometry of the lattice (x_1- and x_2-axis short, x_3-axis long) and with periodic boundary conditions in all three directions of the lattice. In this way sections of ordered and disordered phases are produced along the x_3-axis. So interfaces between disordered and ordered phases can be analyzed.

The structure of this thesis is as follows:
In chapter 2 the theory to describe the Potts model and the interface tension is explained. In chapter 3 the used numerical methods are described. Finally, the results are illustrated in chapter 4 and some conclusions are drawn in chapter 5.

Chapter 2

The Potts model

2.1 Preface

The Potts model is a q-state spin model in d space dimensions. So it is a generalization of the Ising model. According to [10] the Potts model was studied first by the research student Potts in 1951. In 1954 Kihara analyzed the same model independently of Potts. At the beginning nobody was interested in the Potts model. However, later the model was discovered to be very rich in its physical content.
For $q = 2$ the Potts model is equivalent to the Ising model. The number of states $q = 3$ and the space dimension $d = 3$ are used in this master thesis. Therefore every spin can choose between the three directions d_1, d_2, d_3 as shown in figure 2.1. Mathematically the possible

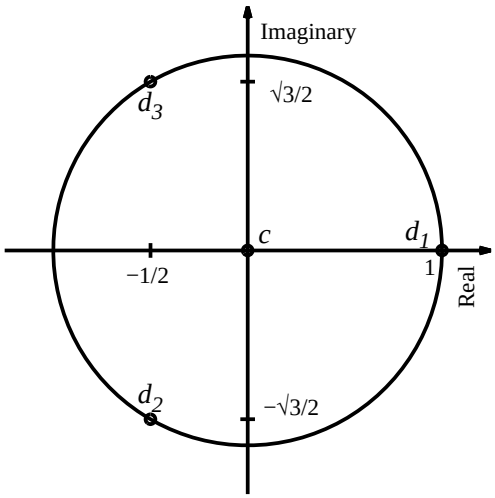

Figure 2.1: Every spin points in one of the directions d_1, d_2, d_3. Parts of the whole system are either in the disordered phase c or in one of the ordered phases d_1, d_2 or d_3.

values of the spin ϕ_x at the lattice point $x = (x_1, x_2, x_3)$ can be expressed as

$$\phi_x \in \mathbb{Z}(3) = \left\{ \mathrm{e}^{k\frac{2\pi i}{3}} \mid k = 0, 1, 2 \right\} \ . \tag{2.1}$$

Then the Hamilton function

$$\mathcal{H} = -\kappa \sum_{\langle xy \rangle} \delta_{(\phi_x, \phi_y)} = -\kappa' \sum_{\langle xy \rangle} \mathsf{RE}\left[\phi_x^* \phi_y\right] \tag{2.2}$$

with $\kappa' = \frac{2}{3}\kappa$ is used. $\sum_{\langle xy \rangle}$ is the sum over the nearest neighbors. The partition function is

$$\mathcal{Z} = \left[\prod_{x'} \sum_{\phi_{x'} \in \mathbb{Z}(3)} \right] \mathrm{e}^{\kappa \sum_{\langle xy \rangle} \ \delta_{(\phi_x, \phi_y)}} \ . \tag{2.3}$$

$\left[\prod_{x'} \sum_{\phi_{x'} \in \mathbb{Z}(3)}\right]$ means that the sum over all possible spin configurations has to be built. Expectation values as, for example, the magnetization are calculated as

$$\langle \Phi \rangle = \frac{1}{\mathcal{Z}} \left[\prod_{x'} \sum_{\phi_{x'} \in \mathbb{Z}(3)} \right] \Phi \ \mathrm{e}^{\kappa \sum_{\langle xy \rangle} \ \delta_{(\phi_x, \phi_y)}} \ , \tag{2.4}$$

where $\Phi = \sum_x \phi_x$.
Assuming a three-dimensional lattice with lengths L_1, L_2 and L_3 and with periodic boundary conditions, correlation functions can be defined in the same way as the magnetization:

$$\langle \widetilde{\mathcal{O}_1}^*(0) \widetilde{\mathcal{O}_1}(x_3) \rangle \quad \text{and} \quad \langle \mathcal{O}_3(0) \mathcal{O}_3(x_3) \rangle \ , \tag{2.5}$$

where

$$\widetilde{\mathcal{O}_1}(x_3) = \frac{1}{L_1 L_2} \sum_{x_1, x_2} \phi_x \quad \text{and} \quad \mathcal{O}_3(x_3) = \frac{1}{L_1^2 L_2^2} \left| \sum_{x_1, x_2} \phi_x \right|^2 \ . \tag{2.6}$$

It is possible to relate the correlation functions to the lowest energy levels of the Hamilton function ($E_{1,2,3}$, assuming $E_0 = 0$). This is done in appendix A and the results are

$$\begin{aligned} \langle \widetilde{\mathcal{O}_1}^*(0) \widetilde{\mathcal{O}_1}(x_3) \rangle &\approx f_1(x_3) \doteq A + B \cosh\left[E_{1,2} \left(\frac{L_3}{2} - x_3 \right) \right] \\ \langle \mathcal{O}_3(0) \mathcal{O}_3(x_3) \rangle &\approx f_3(x_3) \doteq C + D \cosh\left[E_3 \left(\frac{L_3}{2} - x_3 \right) \right] \ , \end{aligned} \tag{2.7}$$

where A, B, C, D are constants depending on L_3. These energy levels, derived from a microscopical interpretation of the lattice, converge to the energy levels in section 2.5, which are derived from a macroscopical interpretation of the lattice, when $L_1 L_2 \to \infty$.

The correlation functions defined in eq.(2.5) and (2.6) are both invariant under rotations and reflections.
The theory of the transfer matrix which is described in [9] is used with the Hamilton function of eq.(2.2). A transfer matrix which describes the microscopical evolution of the spin configuration from one x_1-x_2-plane l to the neighboring x_1-x_2-plane m is defined as

$$\langle \phi^l \mid T \mid \phi^m \rangle = \mathrm{e}^{\frac{\kappa}{2}\sum_{\langle xy\rangle}\delta\left(\phi^l_x,\phi^l_y\right)}\mathrm{e}^{\frac{\kappa}{2}\sum_{\langle xy\rangle}\delta\left(\phi^m_x,\phi^m_y\right)}\mathrm{e}^{\kappa\sum_{\langle xy\rangle}\delta\left(\phi^l_x,\phi^m_y\right)} \ . \tag{2.8}$$

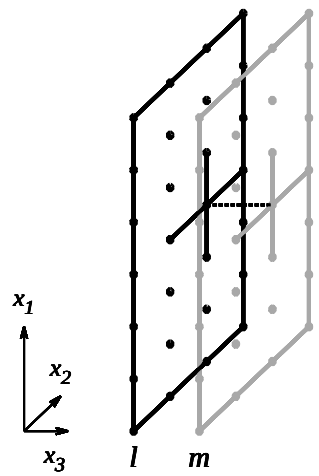

Figure 2.2: This is an illustration how to imagine the transfer matrix on a three-dimensional lattice.

$\langle \phi^l \mid$ resp. $\langle \phi^m \mid$ is the eigenfunction of the spins in the x_1-x_2-plane l resp. m. As illustrated in figure 2.2, the first exponential term of eq.(2.8) is the contribution to the Boltzmann weight of the nearest neighbors in the x_1-x_2-plane l. The second term is the contribution to the Boltzmann weight of the nearest neighbors in the x_1-x_2-plane m. The third exponential term is the contribution to the Boltzmann weight of the nearest neighbors along the x_3-axis between the x_1-x_2-planes l and m. If the trace of T^{L_3} is taken the result is the partition function $\mathcal{Z}$ of eq.(2.3) as shown in appendix B. The transfer matrix has a dimension of $3^{L_1L_2} \times 3^{L_1L_2}$, which is exponentially large for large volumes.

2.2 Symmetries

The Hamilton function defined in eq.(2.2) is invariant under $S_3 = \mathbb{Z}(3) \rtimes \mathbb{Z}(2)$ transformations. $\mathbb{Z}(3)$ corresponds to rotations:

$$\phi_x \to \mathrm{e}^{k\frac{2\pi i}{3}} \phi_x, \quad k = 0, 1, 2 \ . \tag{2.9}$$

$\mathbb{Z}(2)$ corresponds to reflections:

$$\phi_x \to \phi_x^* \ . \tag{2.10}$$

With periodic boundary conditions the Hamilton function of a cubic lattice with size $L_1 L_2 L_3$ is invariant under translations

$$\phi_x \to \phi_{x+\delta x} \quad \text{with} \quad \delta x = (\delta x_1, \delta x_2, \delta x_3) \ . \tag{2.11}$$

2.3 Phases and phase transition

Now we consider a three-dimensional 3-state Potts model, on an infinite lattice. According to [4] in this case there is a phase transition at the critical point $\kappa_c = 0.550565$. When $\kappa < 0.550565$ the system is in the disordered phase c. When $\kappa > 0.550565$ the system is in one of the ordered phases d_1, d_2, d_3. When $\kappa = \kappa_c$ all four phases can be realized by the system. So there is a first order phase transition at κ_c. In the ordered phase, configurations of the system where most of the spins point in the same spontaneously selected direction are more probable than configurations where the spins point in different directions. In the disordered phase the contrary is the case. A system in the disordered phase has $\langle \Phi \rangle = 0$, and the $\mathbb{Z}(3)$ symmetry is not spontaneously broken. A system in one of the ordered phases has $\langle \Phi \rangle \neq 0$. The expectation value of the magnetization $\langle \Phi \rangle$ can pic up three different values depending on the selected phase. Therefore the $\mathbb{Z}(3)$ symmetry is spontaneously broken.

2.4 Wetting

Lipowsky discusses wetting in general and for systems with finite size in [5]. He considers an inhomogeneous system with two coexisting phases α and γ, see figure 2.3 a). Then κ is changed in such a way that the system approaches a critical point where a third phase, β, can coexist with the two phases α and γ. Lipowsky distinguishes between two cases:

- Complete wetting, see figure 2.3 b) : At the critical point, a layer of the β phase appears in the $\alpha\gamma$ interface. The interface tensions satisfy „Antonoff's rule“

$$\sigma_{\alpha\gamma} = \sigma_{\alpha\beta} + \sigma_{\beta\gamma} \ . \tag{2.12}$$

- Incomplete wetting, see figure 2.3 c) : At the critical point the β phase appears at the $\alpha\gamma$ interface as droplets with a finite contact angle φ. The interface tensions satisfy

$$\sigma_{\alpha\gamma} < \sigma_{\alpha\beta} + \sigma_{\beta\gamma} \ . \tag{2.13}$$

The interface tension describes the free energy of an interface.

In a finite system of the three-dimensional 3-state Potts model with short x_1-, x_2-, long x_3-axis and periodic boundary conditions in all three directions, sections of disordered and ordered phases are formed along the x_3-axis at κ_c. So here complete wetting is realized, if an interface between two ordered phases is always separated by a layer of disordered phase. Incomplete wetting is realized, if also direct ordered-ordered interfaces exists with or without droplets of disordered phase in between. In figure 2.4 a configuration of a $21 \times 21 \times 250$ lattice near the critical temperature is plotted.

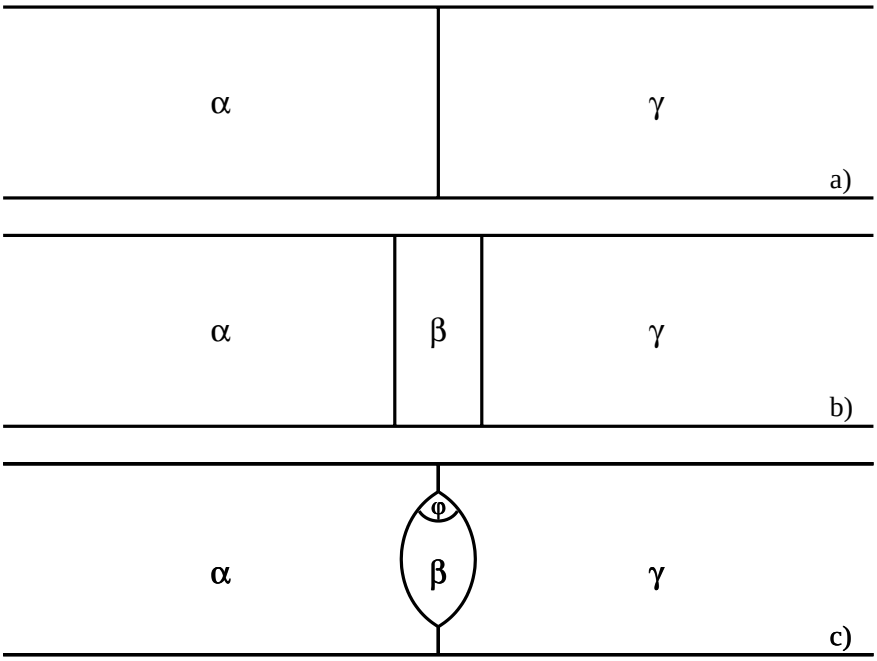

Figure 2.3: Picture a) illustrates the interface between two phases α and β. Picture b) illustrates how complete wetting looks like. Picture c) illustrates how incomplete wetting with droplets looks like.

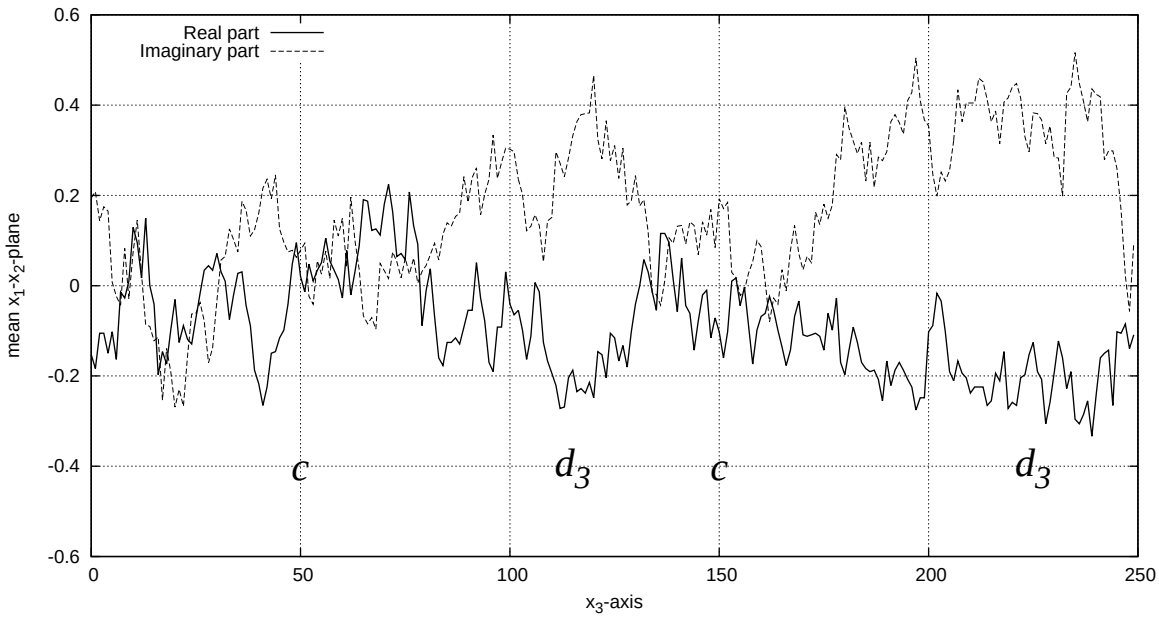

Figure 2.4: Configuration of a $21 \times 21 \times 250$ lattice with $\kappa = 0.55025$. On the ordinate the means of the real and imaginary parts of the spins in the x_1-x_2-plane are plotted. On the abscissa the x_3-axis of the lattice is plotted. The phases (d_3, c) in which lattice sections are assumed to be are noted at the bottom edge.

2.5 The interface tension and the spectrum of the transfer matrix

In order to make the dimension of the transfer matrix of eq.(2.8) smaller, it is interesting to describe the Potts model in a macroscopic way. This description is introduced in [2], where $SU(3)$ pure gauge theory is discussed. It can also be used to describe the lowest states of the transfer matrix of the Potts model. As before, the lattice is a cuboid with one direction (the x_3-axis) much longer than the two others. But now x_1-x_2-planes called interfaces are set along the x_3-axis as separating walls. Between two interfaces the disordered or one of the ordered phases exists. In the complete wetting case there is always a disordered phase section between two ordered phases. In the incomplete wetting case this constraint does not exist. Moreover it is assumed that a block of disordered phase of a thickness x_3^0 costs the free energy $F = f_c A x_3^0$, where f_c is the free energy density of the ordered phase and $A = L_1 L_2$ is the area of a x_1-x_2-plane. Such a block of disordered phase is weighted with a Boltzmann factor

$$\mathrm{e}^{-\frac{F}{T}} = \mathrm{e}^{-\frac{f_c}{T} A x_3^0} \ . \tag{2.14}$$

Similarly, a block of ordered phase gets a factor

$$\mathrm{e}^{-\frac{F}{T}} = \mathrm{e}^{-\frac{f_d}{T} A x_3^0} \ . \tag{2.15}$$

An interface between an ordered and a disordered phase costs the free energy $F = \sigma_{cd} A T$, where σ_{cd} is the reduced disordered-ordered interface tension and T is the temperature. This interface gets the Boltzmann factor

$$\mathrm{e}^{-\frac{F}{T}} = \delta \mathrm{e}^{-\sigma_{cd} A} \ , \tag{2.16}$$

where δ is an A-independent constant.
For such a system the transfer matrix becomes more simple with dimension 4×4

$$t(L_3) = \begin{bmatrix} t_{dd}(L_3) & t_{d'd}(L_3) & t_{dd'}(L_3) & t_{dc}(L_3) \\ t_{dd'}(L_3) & t_{dd}(L_3) & t_{dd'}(L_3) & t_{dc}(L_3) \\ t_{d'd}(L_3) & t_{d'd}(L_3) & t_{dd}(L_3) & t_{dc}(L_3) \\ t_{cd}(L_3) & t_{cd}(L_3) & t_{cd}(L_3) & t_{cc}(L_3) \end{bmatrix} \ . \tag{2.17}$$

For example, the expression $\frac{t_{dd}(L_3)}{\mathrm{Tr}[t(L_3)]}$ is the probability of a lattice with length L_3 to have $x_3 = 0$ and $x_3 = L_3$ in a section of ordered phase. Figure 2.5 shows how the matrix elements can be described graphically in the complete wetting case.

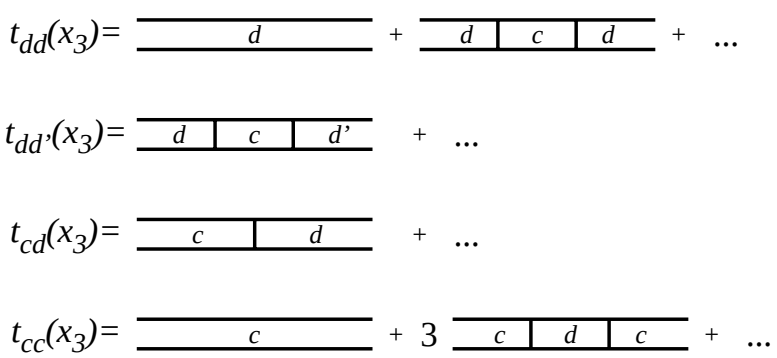

Figure 2.5: Graphical description of the transfer matrix elements in the effective interface model for the complete wetting case

With the defined Boltzmann factors of eq.(2.14)-(2.16) these matrix elements and the eigenvalues of the transfer matrix can be calculated, as it was done in [2]. Here just the results with $X \doteq \frac{1}{2}(f_c - f_d) A/T$ and $\delta' \doteq \sqrt{3}\delta \mathrm{e}^{-\sigma_{cd} A}$ are given:

$$t_0(L_3) = \mathrm{e}^{L_3 \sqrt{X^2 + \delta'^2}} \ , \quad t_{1,2}(L_3) = \mathrm{e}^{L_3 X} \ , \quad t_3(L_3) = \mathrm{e}^{-L_3 \sqrt{X^2 + \delta'^2}} \tag{2.18}$$

are the eigenvalues of the transfer matrix. With the energy levels of this system defined as

$$t_i \doteq \mathrm{e}^{-E_i L_3} \ , \tag{2.19}$$

the energy differences

$$E_{1,2} - E_0 = \sqrt{X^2 + 3\delta^2 \mathrm{e}^{-2\sigma_{cd}A}} - X \ , \quad E_3 - E_0 = 2\sqrt{X^2 + 3\delta^2 \mathrm{e}^{-2\sigma_{cd}A}} \tag{2.20}$$

result. The energy differences have a minimum at $X = 0$. This is at the critical temperature, where $f_c = f_d$

$$E_{1,2} - E_0 = \sqrt{3\delta^2 \mathrm{e}^{-\sigma_{cd}A}} \ , \quad E_3 - E_0 = 2\sqrt{3\delta^2 \mathrm{e}^{-\sigma_{cd}A}} \ . \tag{2.21}$$

At the critical temperature it obviously follows that

$$2(E_{1,2} - E_0) = E_3 - E_0 \ . \tag{2.22}$$

As for the complete wetting case it is possible to construct a transfer matrix for the incomplete wetting case as well. In that case direct interfaces between two ordered phases exist with an interface tension σ_{dd}. The minimum of the energy difference

$$E_3 - E_0 = \sqrt{(X + \gamma \mathrm{e}^{-\sigma_{dd}A})^2 + 3\delta^2 \mathrm{e}^{-2\sigma_{cd}A}} \tag{2.23}$$

no longer occurs at the critical temperature. In the incomplete wetting case the minimum is at $X = -\gamma \mathrm{e}^{-\sigma_{dd}A} < 0$ which lies in the disordered phase. The point of the equidistant energy splittings between the lowest levels, $2(E_{1,2} - E_0) = E_3 - E_0$ with

$$E_{1,2} - E_0 = \sqrt{(X + \gamma \mathrm{e}^{-\sigma_{dd}A})^2 + 3\delta^2 \mathrm{e}^{-2\sigma_{cd}A}} - X + 2\gamma \mathrm{e}^{-\sigma_{dd}A} \ , \tag{2.24}$$

is now at $X = 2\gamma \mathrm{e}^{-\sigma_{dd}A} > 0$ which lies in the ordered phase. γ is a constant. The detailed calculations are performed in [2].

Chapter 3

Numerical simulation

3.1 The Monte Carlo method

This section follows [1] and [9].
On large lattices the partition function in eq.(2.3) is represented by an extremely large sum. With the Monte Carlo method configurations are generated with the same distribution as they would occur in the partition function. Instead of calculating expectation values by building extremely large sums, estimators of the expectation value can be computed using the configurations generated with the Monte Carlo method. In a Monte Carlo simulation the configuration k_{n+1} is generated stochastically from a configuration k_n, so that no information about previous configurations k_{n-1}, k_{n-2},... is needed. This time sequence is called a Markov chain and the elements of it are the configurations. A sufficiently large number of steps after the initial configuration k_1, an equilibrium distribution is reached by the Monte Carlo algorithm.
If the Monte Carlo algorithm fulfills

a) Ergodicity: Starting from an arbitrary initial configuration the algorithm can, at least in principle, reach any other configuration.

b) Normalization: $\sum_{\mathcal{C}'} W\left[\mathcal{C} \to \mathcal{C}'\right] = 1$, where $\mathcal{C}$ and $\mathcal{C}'$ are configurations and $W\left[\mathcal{C} \to \mathcal{C}'\right]$ is the probability to reach the configuration $\mathcal{C}'$ from configuration $\mathcal{C}$.

c) Detailed Balance (with eq.(2.2), more general see [9] or [1]):

$$W[\mathcal{C} \to \mathcal{C}']\mathrm{e}^{\kappa \sum_{\langle xy \rangle_{\mathcal{C}}} \delta_{(\phi_x, \phi_y)}} = W[\mathcal{C}' \to \mathcal{C}]\mathrm{e}^{\kappa \sum_{\langle xy \rangle_{\mathcal{C}'}} \delta_{(\phi_x, \phi_y)}} , \tag{3.1}$$

it converges to the correct equilibrium distribution.

3.2 The Swendsen-Wang cluster algorithm

3.2.1 Description of the simulation

In this work the Swendsen-Wang multi-cluster algorithm of [7] is used to simulate the 3-state Potts model in three dimensions. First, a three-dimensional lattice is built with a spin at each lattice point. In this case the spins are in one of three possible states (0,1,2). To switch some spins in the lattice, clusters are constructed. For this purpose a sweep through all lattice points is realized. In this sweep bonds between neighboring spins with the same state are activated with a probability of

$$p = 1 - \mathrm{e}^{-\kappa} \ . \tag{3.2}$$

Between neighboring spins which are not in the same state no bond is activated. In a second sweep all spins which are connected by an activated bond are united in clusters. The first lattice point is taken. Then it is checked if this point already belongs to a cluster. If it does not, it is the first point in a new cluster. If there exist neighbors of this point connected by an activated bond they are also added to the same cluster. Then it has to be checked if there exist neighbors of the added neighbors with activated bonds and so on. When a cluster is completed the second lattice point is taken. It is checked if it already belongs to a cluster. If it does not, it is the first point in a new cluster. And the whole process described above starts again until all lattice points are associated with a cluster. There exist also clusters including just one lattice point. During the same sweep the spins of every cluster get a (new) state with the probability of 1/3 for every state. After this procedure a new spin configuration is generated. The estimators are measured during the second sweep.
In this thesis the detailed instructions of exercise 6.3 in [8] are followed.

3.2.2 Ergodicity

There exists always the possibility with non-vanishing probability to have every lattice point associated with a different cluster and therefore to flip every spin independent of its neighbors. So for every starting configuration it is possible with non-vanishing probability to reach every possible spin configuration even in one step. This makes the multi-cluster algorithm ergodic.

3.2.3 Normalization

	probability of activated bond	**probability of inactivated bond**
parallel spins	$\mathrm{e}^{-\kappa}$	$(1 - \mathrm{e}^{-\kappa})$
not parallel spins	1	0

Table 3.1: List of probabilities to activate bonds

Beginning with a spin configuration $\mathcal{C}$ a new spin configuration $\mathcal{C}'$ is constructed. The number of pairs of neighboring sites with parallel spins is $h(\mathcal{C})$. The set $\mathcal{M}$ includes the different ways to activate bonds in the spin configuration $\mathcal{C}$ so that configuration $\mathcal{C}'$ can be generated. $m \in \mathcal{M}$ is a possible distribution of activated bonds. a is the number of activated bonds between parallel and neighboring spins. The activated bonds implicate a cluster number $N_{\text{Cluster}}(m)$. Every cluster gets a (new) spin state with the probability 1/3. The probability to generate the configuration $\mathcal{C}'$ out of $\mathcal{C}$ then is

$$W[\mathcal{C} \to \mathcal{C}'] = \sum_{m \in \mathcal{M}} \underbrace{\left(1 - \mathrm{e}^{-\kappa}\right)^{a(m)} \mathrm{e}^{-(h(\mathcal{C}) - a(m))\kappa}}_{\text{Probability of a particular bond distribution}} \underbrace{\left(\frac{1}{3}\right)^{N_{\text{Cluster}}(m)}}_{\text{Probability to flip the clusters}} . \tag{3.3}$$

Then

$$\begin{aligned}
\sum_{\mathcal{C}'} W[\mathcal{C} \to \mathcal{C}'] &= \sum_{\mathcal{C}'} \sum_{m \in \mathcal{M}} \left(1 - \mathrm{e}^{-\kappa}\right)^{a(m)} \mathrm{e}^{-(h(\mathcal{C}) - a(m))\kappa} \left(\frac{1}{3}\right)^{N_{\text{Cluster}}(m)} \\
&= \sum_{a=0}^{h(\mathcal{C})} \sum_{m \in \mathcal{M}(a)} 3^{N_{\text{Cluster}}(m)} \left(1 - \mathrm{e}^{-\kappa}\right)^{a} \mathrm{e}^{-(h(\mathcal{C}) - a)\kappa} \left(\frac{1}{3}\right)^{N_{\text{Cluster}}(m)} \\
&= \sum_{a=0}^{h(\mathcal{C})} \binom{h(\mathcal{C})}{a} \left(1 - \mathrm{e}^{-\kappa}\right)^{a} \mathrm{e}^{-(h(\mathcal{C}) - a)\kappa} \\
&= 1 \, . \qquad (3.4)
\end{aligned}$$

The factor $\binom{h(\mathcal{C})}{a}$ comes in because $\mid \mathcal{M}(a) \mid = \binom{h(\mathcal{C})}{a}$.

3.2.4 Detailed balance

Using section 3.1 and multiplying eq.(3.3) by the Boltzmann weight of the corresponding spin configuration, it can be seen that detailed balance is realized:

$$\begin{aligned}
W[\mathcal{C} \to \mathcal{C}'] \mathrm{e}^{\kappa \sum_{\langle xy \rangle_{\mathcal{C}}} \delta_{(\phi_x, \phi_y)}} &= \sum_{\mathcal{M}} (1 - \mathrm{e}^{-\kappa})^{a(\mathcal{M})} \mathrm{e}^{-(h(\mathcal{C}) - a(\mathcal{M}))\kappa} \mathrm{e}^{h(\mathcal{C})\kappa} \left[\frac{1}{3}\right]^{N_{\text{Cluster}}} \\
&= \sum_{\mathcal{M}} (1 - \mathrm{e}^{-\kappa})^{a(\mathcal{M})} \mathrm{e}^{a(\mathcal{M})\kappa} \left[\frac{1}{3}\right]^{N_{\text{Cluster}}} \\
W[\mathcal{C}' \to \mathcal{C}] \mathrm{e}^{\kappa \sum_{\langle xy \rangle_{\mathcal{C}'}} \delta_{(\phi_x, \phi_y)}} &= \sum_{\mathcal{M}'} (1 - \mathrm{e}^{-\kappa})^{a'(\mathcal{M}')} \mathrm{e}^{-(h'(\mathcal{C}') - a'(\mathcal{M}'))\kappa} \mathrm{e}^{h'(\mathcal{C}')\kappa} \left[\frac{1}{3}\right]^{N_{\text{Cluster}}} \\
&= \sum_{\mathcal{M}'} (1 - \mathrm{e}^{-\kappa})^{a'(\mathcal{M}')} \mathrm{e}^{a'(\mathcal{M}')\kappa} \left[\frac{1}{3}\right]^{N_{\text{Cluster}}} \qquad (3.5)
\end{aligned}$$

$\sum_{\langle xy\rangle_{\mathcal{C}}} \delta_{(\phi_x,\phi_y)}$ is the sum over the nearest neighbors in the spin configuration $\mathcal{C}$. Constructing $\mathcal{C}'$ out of $\mathcal{C}$ implies $\mathcal{M}' = \mathcal{M}$. Therefore $a(\mathcal{M})$ is equal to $a'(\mathcal{M}')$ and

$$W[\mathcal{C} \to \mathcal{C}']\mathrm{e}^{\kappa \sum_{\langle xy\rangle_{\mathcal{C}}} \delta_{(\phi_x,\phi_y)}} = W[\mathcal{C}' \to \mathcal{C}]\mathrm{e}^{\kappa \sum_{\langle xy\rangle_{\mathcal{C}'}} \delta_{(\phi_x,\phi_y)}} \ . \tag{3.6}$$

Because of ergodicity and detailed balance the equilibrium distribution is unique according to page 67 of [9].

3.3 Estimators

With the Monte Carlo simulation estimators of the correlation functions (2.5), (2.6) are measured. In the case of $\langle \mathcal{O}_3(0)\mathcal{O}_3(x_3)\rangle$ for every simulated spin configuration just

$$\frac{1}{L_3}\sum_{x_3'=0}^{L_3-1} \mathcal{O}_3(x_3')\mathcal{O}_3(x_3'+x_3)$$

is calculated as an unimproved estimator. In the same way the unimproved estimator of $\langle \widetilde{\mathcal{O}_1}^*(0)\widetilde{\mathcal{O}_1}(x_3)\rangle$ can be calculated. However, it is possible to construct an improved estimator of $\langle \widetilde{\mathcal{O}_1}^*(0)\widetilde{\mathcal{O}_1}(x_3)\rangle$. It is possible to define the function $\mathrm{CL}(\phi_x)$. The value of this function is the cluster which ϕ_x belongs to. The probability to pick up a particular value in $\mathbb{Z}(3)$ is $1/3$ for every spin $\phi(x_1,x_2,x_3) = \phi_x$. Then the distributions and the expectation values of $\phi^r(x_1,x_2,0)\phi^r(x_1',x_2',x_3)$ and $\phi^i(x_1,x_2,0)\phi^i(x_1',x_2',x_3)$ for the cases „both spins in the same cluster“ and „both spins in different clusters“ can be calculated. The expectation values of both expressions for the case „both spins in the same cluster“ are $1/2$ and 0 for the case „both spins in different clusters“. With $\langle \phi^i(x_1,x_2,0)\phi^r(x_1',x_2',x_3)\rangle = \langle \phi^i(x_1,x_2,0)\rangle\langle \phi^r(x_1,x_2,0)\rangle$ it results

$$\begin{aligned}
\langle \phi^*(x_1,x_2,0)\phi(x_1',x_2',x_3)\rangle &= \langle \phi^r(x_1,x_2,0)\phi^r(x_1',x_2',x_3)\rangle + \langle \phi^i(x_1,x_2,0)\phi^i(x_1',x_2',x_3)\rangle \\
&= \begin{cases} 1 & \text{if both spins are in the same cluster} \\ 0 & \text{if the spins are in different clusters} \end{cases} \\
&= \delta_{\mathrm{CL}(\phi(x_1,x_2,0)),\mathrm{CL}\left(\phi(x_1',x_2',x_3)\right)} \ .
\end{aligned} \tag{3.7}$$

Then the improved estimator of

$$\langle \widetilde{\mathcal{O}_1}^*(0)\widetilde{\mathcal{O}_1}(x_3)\rangle = \left[\frac{1}{L_1L_2}\right]^2 \sum_{x_1,x_2,x_1',x_2'} \langle \phi^*(x_1,x_2,0)\phi(x_1',x_2',x_3)\rangle \tag{3.8}$$

is calculated with

$$\frac{1}{L_3}\sum_{x_3'=0}^{L_3-1}\delta_{\mathrm{CL}(\phi(x_1,x_2,0)),\mathrm{CL}\left(\phi(x_1',x_2',x_3)\right)} \tag{3.9}$$

for every simulated spin configuration. The improved estimator takes all possible spin configurations with the same cluster distribution as the given spin configuration into account. Therefore the improved estimator is expected to be more accurate than the unimproved one. In section 4.3 unimproved and improved estimators are compared to each other.

3.4 Data analysis

3.4.1 How to fit the Monte Carlo Data

The estimators of $\langle\widetilde{\mathcal{O}_1}^*(0)\widetilde{\mathcal{O}_1}(x_3)\rangle$ and $\langle\mathcal{O}_3(0)\mathcal{O}_3(x_3)\rangle$ are measured by the simulation program as described in section 3.3. The simulation program writes $N = 2^{12}$ times the mean of 2^8 measurements $\{\mathsf{corr}_{1,3}(x_3)\}_{i=1}^N$ in a txt-file for a given lattice and a given κ-value. Then jackknife samples (following [11]) are built out of these measurements

$$\mathsf{corr}^J_{1,3_{(i)}}(x_3) = \frac{1}{N-1}\sum_{\substack{k=1\\k\neq i}}^{N}\mathsf{corr}_{1,3_{(k)}}(x_3)\ . \tag{3.10}$$

In order to obtain the estimators of the energies $E_{1,2}$ and E_3 the functions $f_{1,3}(x_3)$ of eq.(2.7) are fitted for $\{\mathsf{corr}^J_{1,3}(x_3)\}_{i=1}^N$. The results of this procedure are jackknife samples $\{E^J_{1,2}\}_{i=1}^N$ and $\{E^J_3\}_{i=1}^N$ of estimators for the energies $E_{1,2}$ and E_3. The jackknife estimators and the uncertainties of $E_{1,2}$ and E_3 are computed with

$$\overline{E^J_{1,2,3}} = \frac{1}{N}\sum_{i=1}^{N}E^J_{1,2,3_{(i)}}\ ,\quad \delta^{\overline{E}}_{1,2,3} = \sqrt{(N-1)\left[\overline{(E^J_{1,2,3})^2} - \left(\overline{E^J_{1,2,3}}\right)^2\right]}\ . \tag{3.11}$$

That calculation is based on [11] as well.
The fit is done by minimizing

$$\chi^2_{1,3} = \sum_{x_3'=x_3^{\mathrm{begin}}}^{x_3^{\mathrm{end}}}\left[\mathsf{corr}^J_{1,3}(x_3') - f_{1,3}(x_3')\right]^2\ . \tag{3.12}$$

The way how to fix x_3^{begin} and x_3^{end} is explained in section 3.4.2. In order to get the jackknife samples of the estimators of the energies, the evaluation program runs through a chosen spectrum of possible energy values around the roughly estimated energy values $E^{\mathrm{rough}}_{1,2,3}$ described in section 3.4.2. For every value the constant A is fixed with $\frac{\partial\chi^2_1}{\partial A} = 0$, the other constants are

calculated in the same way. For every value the program computes $\chi^2_{1,3}$. It takes the energy value which has the smallest $\chi^2_{1,3}$ to set a new and finer energy spectrum to run trough. This procedure is repeated until the criterion

$$\frac{\chi^2_{1,3_{\text{old}}} - \chi^2_{1,3_{\text{new}}}}{\chi^2_{1,3_{\text{old}}}} < 10^{-10} \tag{3.13}$$

is fulfilled.

3.4.2 Rough estimator of $E_{1,2}$ and E_3

The functions

$$m_{1,3}(x_3) = \ln\left[\frac{\mathsf{corr}_{1,3}(x_3) - \mathsf{corr}_{1,3}(x_3+1)}{\mathsf{corr}_{1,3}(x_3+1) - \mathsf{corr}_{1,3}(x_3+2)}\right] \quad \text{(new)} \tag{3.14}$$

are constructed. If $x_3 \ll \frac{L_3}{2}$ and if x_3 is large enough so that higher energy effects are negligible then $m_{1,3}(x_3)$ can be taken as an estimator of $E_{1,2,3}$. Because the functions $f_1(x_3)$ and $f_3(x_3)$ of eq.(2.7) have the feature

$$\begin{aligned} \ln\left[\frac{f_1(x_3) - f_1(x_3+1)}{f_1(x_3+1) - f_1(x_3+2)}\right] &\overset{x_3 \ll L_3/2}{\longrightarrow} E_{1,2} \ , \\ \ln\left[\frac{f_3(x_3) - f_3(x_3+1)}{f_3(x_3+1) - f_3(x_3+2)}\right] &\overset{x_3 \ll L_3/2}{\longrightarrow} E_3 \ . \end{aligned} \tag{3.15}$$

Looking at the plot of $m_1(x_3)$ in figure 3.1 (new), the region where $m_1(x_3)$ can be taken as an estimator of $E_{1,2}$ is characterized by a plateau. x_3^{begin} and x_3^{end} are the beginning and ending points of this plateau. The same could be done for $m_3(x_3)$. The rough estimator $E^{\text{rough}}_{1,2,3}$ which is used for the fitting procedure in section 3.4.1 is computed by

$$E^{\text{rough}}_{1,2,3} = \frac{1}{x_3^{\text{end}} - x_3^{\text{begin}} + 1} \sum_{x_3' = x_3^{\text{begin}}}^{x_3^{\text{end}}} m_{1,3}(x_3') \ . \tag{3.16}$$

If the constants A or C are zero, the functions

$$m_{1,3}(x_3) = \ln\left[\frac{\mathsf{corr}_{1,3}(x_3)}{\mathsf{corr}_{1,3}(x_3+1)}\right] \quad \text{(conventional)} \tag{3.17}$$

can be used instead of the functions in eq.(3.14).
For a $17 \times 17 \times 250$ lattice at $\kappa = 0.54875$ the constant A is zero (constant C is not). In this case both calculations, conventional and new, are valid. This is illustrated in figure 3.1. The starting and ending points of the plateau are set at $x_3^{\text{begin}} = 15$ and $x_3^{\text{end}} = 50$ and the fit (described in section 3.4.1) is shown in figure 3.2.

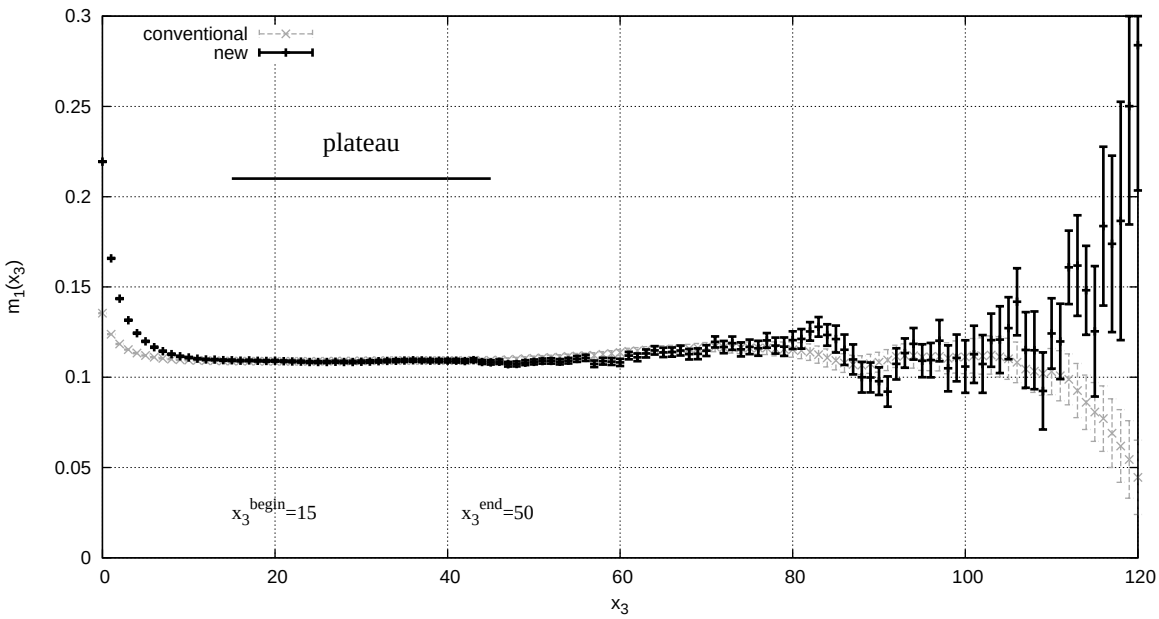

Figure 3.1: Comparision of the two ways to estimate the plateaus for a $17 \times 17 \times 250$ lattice at $\kappa = 0.54875$

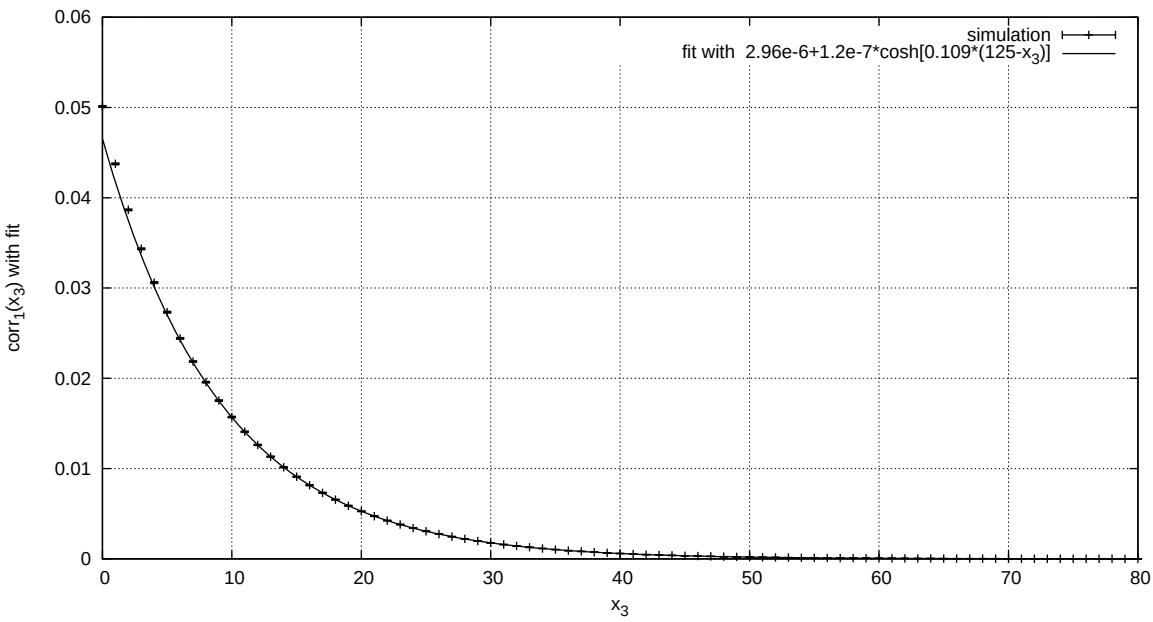

Figure 3.2: $\mathsf{corr}_1(x_3)$ of a $17 \times 17 \times 250$ lattice at $\kappa = 0.54875$

Chapter 4

Numerical results

4.1 Comparison of the analytical solution and the simulation results

There exist $3^{2^3} = 6561$ possible lattice configurations for a 2^3 lattice. For this lattice size it is possible to calculate the exact values of the expectation values $\langle \widetilde{\mathcal{O}_1}^*(0)\widetilde{\mathcal{O}_1}(0)\rangle$, $\langle \widetilde{\mathcal{O}_1}^*(0)\widetilde{\mathcal{O}_1}(1)\rangle$, $\langle \mathcal{O}_3(0)\mathcal{O}_3(0)\rangle$, $\langle \mathcal{O}_3(0)\mathcal{O}_3(1)\rangle$ in order to compare them to the estimated results of the simulation. For example

$$\langle \widetilde{\mathcal{O}_1}^*(0)\widetilde{\mathcal{O}_1}(0)\rangle = \frac{1}{\mathcal{Z}} \left[\prod_{x'} \sum_{\phi_{x'} \in \mathbb{Z}(3)} \right] \widetilde{\mathcal{O}_1}^*(0)\widetilde{\mathcal{O}_1}(0)\ \mathrm{e}^{\kappa \sum_{\langle xy \rangle}\ \delta_{(\phi_x, \phi_y)}}\ . \tag{4.1}$$

This is done for 2^{20} measurements and for κ-values between 0.4 and 0.6. In figure 4.1 most of the expectation values lie within the error bars of the simulated estimators. This shows that the simulation program works correctly.

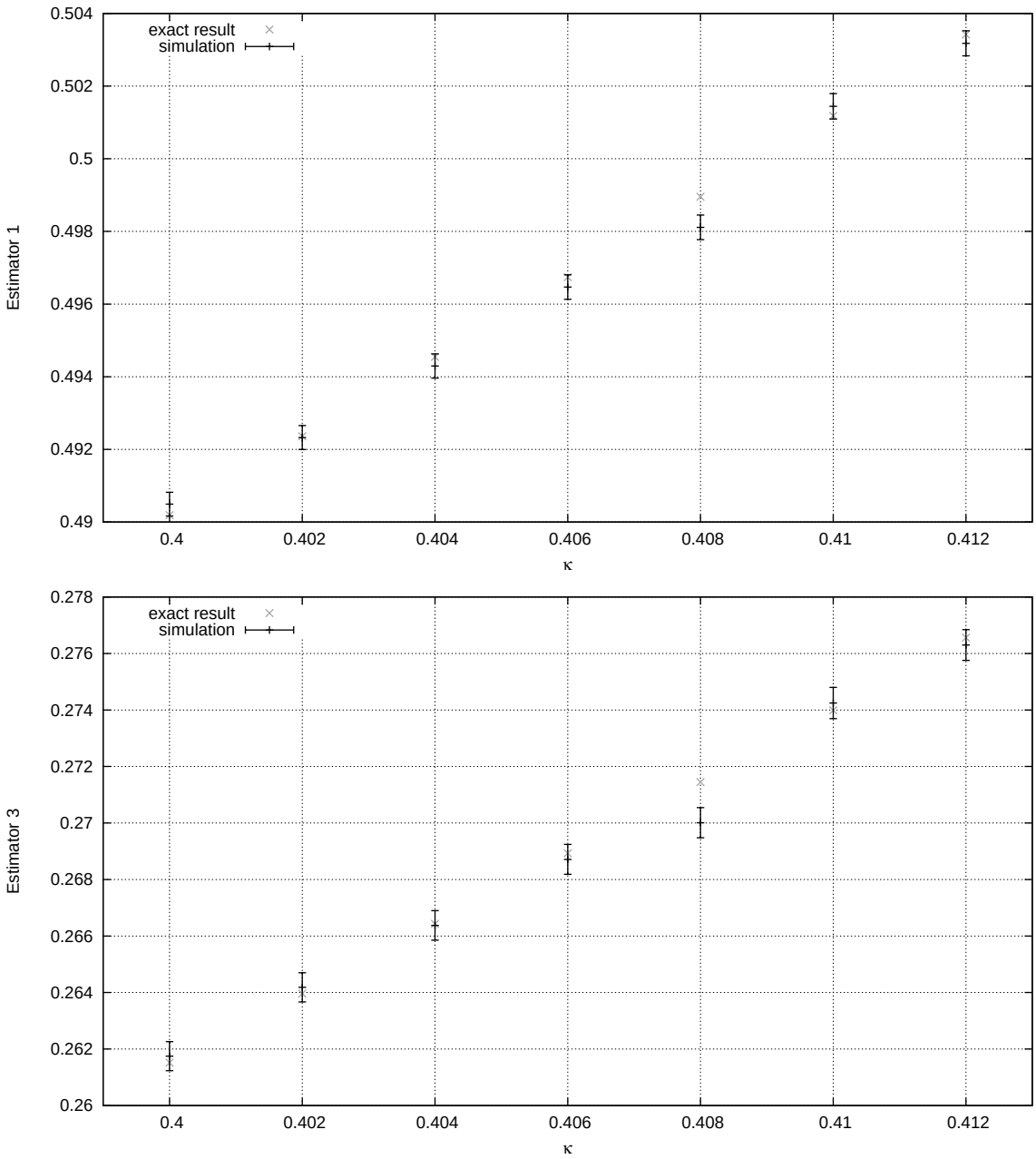

Figure 4.1: Comparison of exact and simulated results of the estimators for $\kappa \in [0.4, 0.412]$ for a 2^3 lattice.
The estimator of $\langle \widetilde{\mathcal{O}_1}^*(0)\widetilde{\mathcal{O}_1}(0)\rangle$ resp. the estimator of $\langle \mathcal{O}_3(0)\mathcal{O}_3(1)\rangle$ is identified by „Estimator 1“ resp. „Estimator 3“.

4.2 Comparison with independent results

In figure 4.2 the independent results obtained by Erik Nygren [6] and the results of this thesis are plotted. The results of both simulations lie within the error bars of each other. The

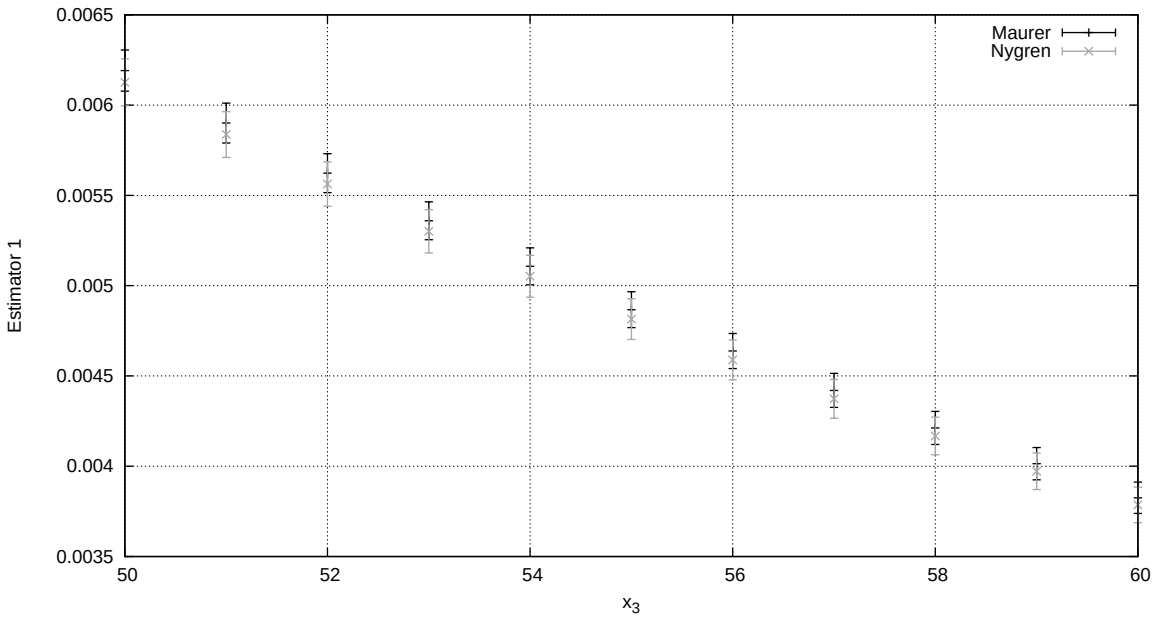

Figure 4.2: Plot of the estimator of $\langle \widetilde{\mathcal{O}_1}^*(0)\widetilde{\mathcal{O}_1}(x_3)\rangle$ (Estimator 1) on a $20 \times 20 \times 250$ lattice at $\kappa = 0.5502$

gray resp. the black measurements are done during one single simulation. Therefore the gray resp. the black measurements are correlated internally. This explains why all of the gray measurements lie a little bit below the black measurements.

4.3 Comparison of the improved and unimproved estimators

κ	$x_3 = 0$ improved	$x_3 = 0$ unimproved	$x_3 = 1$ improved	$x_3 = 1$ unimproved
0.4	0.4905(3)	0.4905(5)	0.2501(5)	0.2497(6)
0.45	0.5488(4)	0.5491(5)	0.3309(6)	0.3309(8)
0.5	0.6138(5)	0.6137(6)	0.4245(7)	0.4240(9)
0.55	0.6825(5)	0.6824(6)	0.5256(8)	0.5256(9)
0.6	0.7496(5)	0.7495(6)	0.6254(8)	0.6254(10)

Table 4.1: Comparison of improved and unimproved estimators

In table 4.1 unimproved and improved estimators of $\langle \widetilde{\mathcal{O}_1}^*(0)\widetilde{\mathcal{O}_1}(x_3)\rangle$ $(x_3 = 0, 1)$ are compared with each other for different κ-values on a 2^3 lattice. As expected, the improved estimator is more accurate than the unimproved one. But here the improvement is marginal. It depends on the lattice size and the κ-value.

4.4 The energies measured at different κ-values

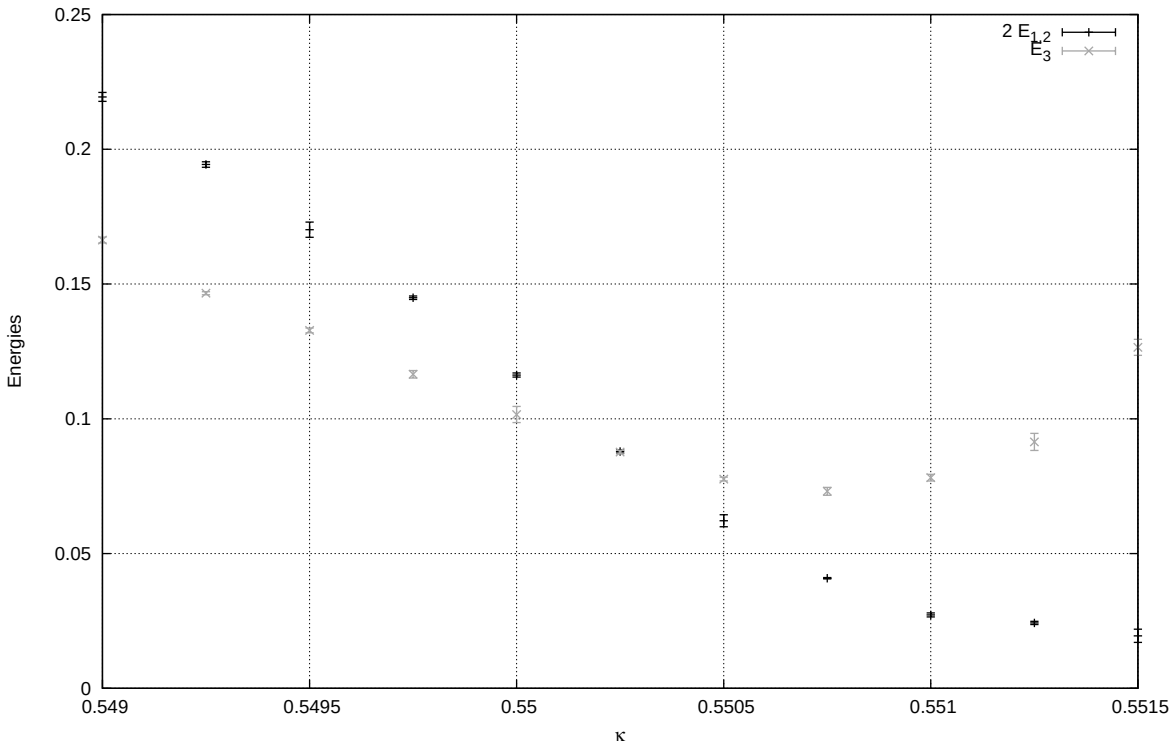

Figure 4.3: Plot of the energy values of a $21 \times 21 \times 250$ lattice

The lowest energy eigenvalues of the transfer matrix on a 21×21 ($\times 250$) lattice are plotted in figure 4.3. The eigenvalues are independent of the size of the lattice in the x_3-direction. As discussed in section 2.5, if incomplete wetting should be realized the equidistant energy splitting would lie in the ordered phase and the minimum of E_3 ($E_0 = 0$) would lie in the disordered phase. Therefore in the plot, first the minimum of E_3 and then the intersection point between $2E_{1,2}$ and E_3 should occur from left to right. However, in figure 4.3 it is the other way around. This is an indication that in the Potts model with periodic boundary conditions complete wetting is realized. According to section 2.5 the minimum of E_3 and the intersection point between $2E_{1,2}$ and E_3 should occur at the same κ. This is not the case in figure 4.3. The same effect has also been measured in [2]. It can be interpreted as a sub-leading finite-size effect which is not correctly reproduced by the calculations done in section 2.5.
Eq.(A.6) and (A.7) predict, that the estimator of $\langle \widetilde{\mathcal{O}_1}^*(0)\widetilde{\mathcal{O}_1}(x_3)\rangle$ for large L_3 should go to zero at $x_3 = L_3/2$. Looking at figure 4.4 it is obvious that this is not the case for $\kappa \geq 0.5505$. So $L_3 = 250$ is too small for $\kappa > 0.5505$. Therefore it is possible that $E_{1,2,3}$ are not estimated properly with the functions in eq.(2.7) when $\kappa > 0.5505$ and $L_3 = 250$.
For lattices with $A = 20^2, 21^2, 22^2$ the estimator is $\langle \widetilde{\mathcal{O}_1}^*(0)\widetilde{\mathcal{O}_1}(125)\rangle \sim 10^{-3}$ and for lattices with $A = 27^2, 29^2, 31^2$ the estimator is $\langle \widetilde{\mathcal{O}_1}^*(0)\widetilde{\mathcal{O}_1}(125)\rangle \sim 10^{-2}$.

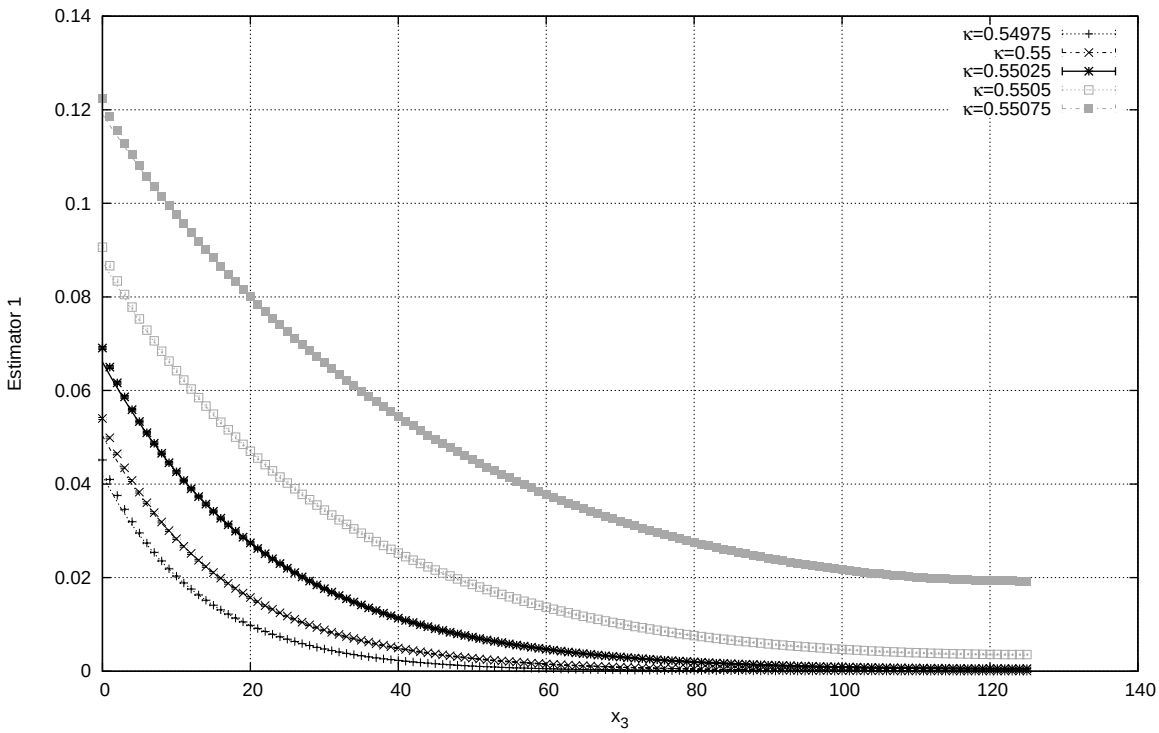

Figure 4.4: Plot of the estimator of $\langle \widetilde{\mathcal{O}_1}^*(0)\widetilde{\mathcal{O}_1}(x_3)\rangle$ (Estimator 1) on a $21 \times 21 \times 250$ lattice at different κ-values.

In [2] for a $20 \times 20 \times 120$ lattice with $\kappa = 0.5502$ $E_{1,2} = 0.048(1)$ has been calculated. In this work for the same κ-value and lattice $E_{1,2} = 0.0493(3)$ has been calculated. Both results match together within the error bars. But looking at figure 4.5 it seems that $L_3 = 120$ is too short. Therefore $E_{1,2} = 0.0491(3)$ has been calculated for a $20 \times 20 \times 250$ lattice at the same κ-value in this work. Within the error bars this result is consistent with the other two before. This is why $L_3 = 120$ is large enough.

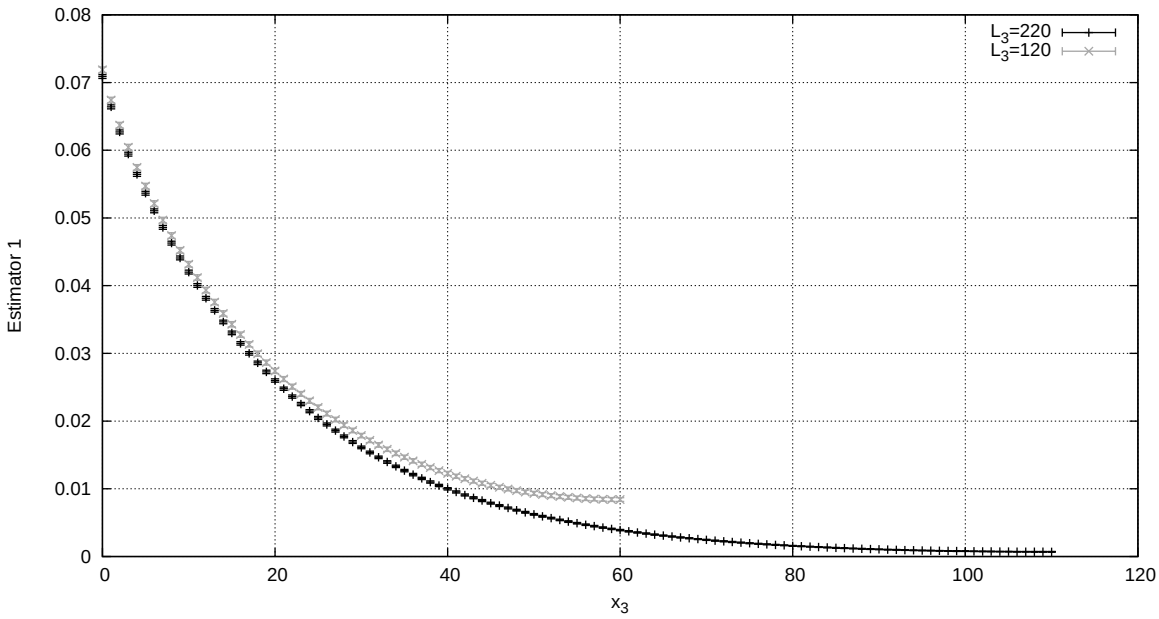

Figure 4.5: Estimator 1 represents the estimator of $\langle \widetilde{\mathcal{O}_1}^*(0)\widetilde{\mathcal{O}_1}(x_3)\rangle$ of two lattices with $A = 20^2$ and $\kappa = 0.5502$.

4.5 The interface tension σ_{cd}

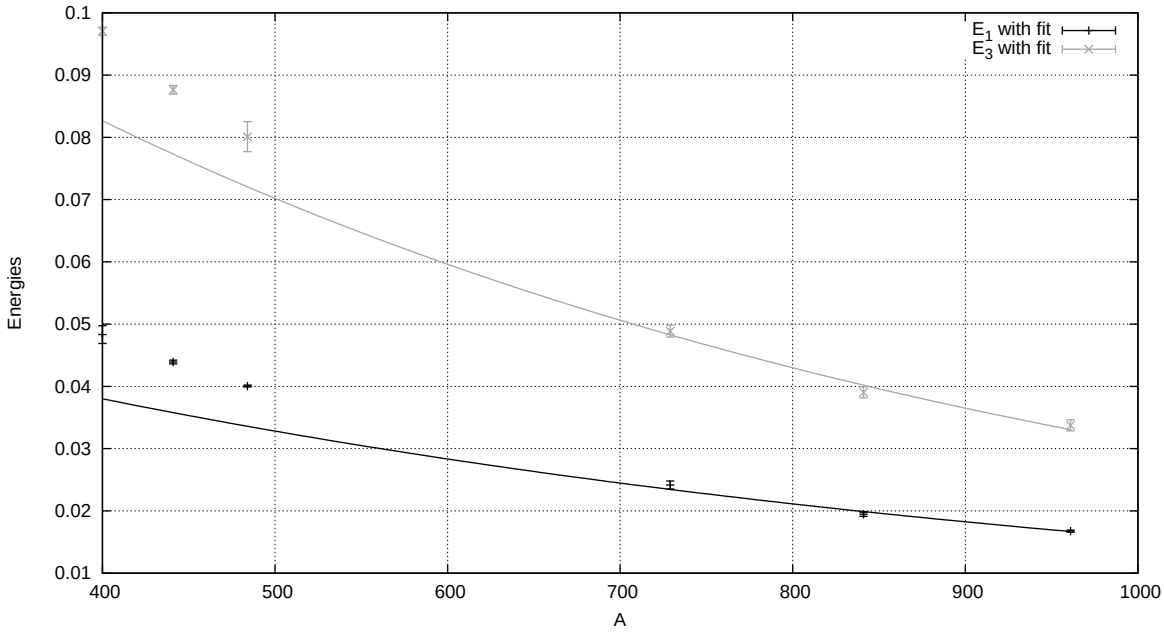

Figure 4.6: The energy values at the critical κ-value as a function of the lattice cross-section A are plotted. The fit is done only with the energies where $A \in [700, 1000]$.

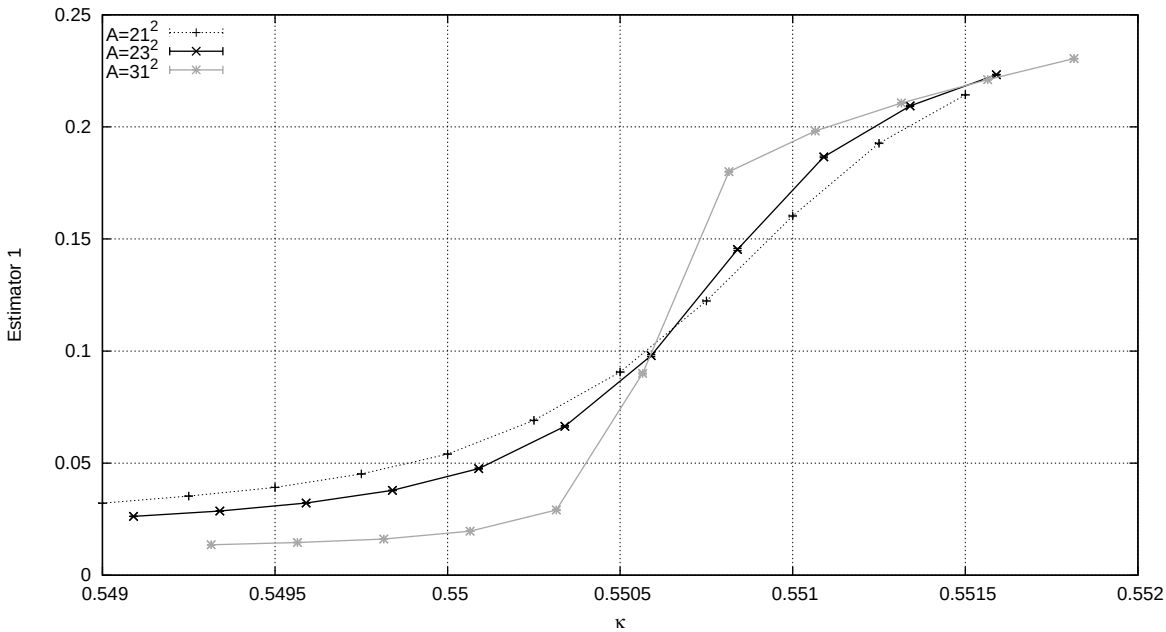

Figure 4.7: Illustration of the dependence of the κ interval where the phase transition occurs on A. Plotted is the estimator of $\langle \widetilde{\mathcal{O}_1}^*(0)\widetilde{\mathcal{O}_1}(0)\rangle$ (Estimator 1).

The energy eigenvalues associated with different lattice cross-sections A at the critical κ-value are plotted in figure 4.6. The critical κ is assumed to be the value where $2E_{1,2} = E_3$ (with $E_0 = 0$) is valid. Theoretically the results should be describable with the functions of eq.(2.21). The fit is done with gnuplot. Using the Marquardt-Levenberg algorithm the sum of the squared residuals weighted by their deviation is minimized. Putting the fit through all six points (see figure 4.6) it results for E_1

$$\sigma_{cd} = 0.00188(5) \quad \text{with} \quad \frac{\chi^2}{\text{d.o.f}} = 5.19 \ , \tag{4.2}$$

and for E_3

$$\sigma_{cd} = 0.00199(6) \quad \text{with} \quad \frac{\chi^2}{\text{d.o.f}} = 3.24 \ . \tag{4.3}$$

Figure 4.7 shows, that the phase transition for lattices with small A occurs within a pseudo-critical region of the κ-value. So maybe σ_{cd} is not estimated well by putting a fit through results with small A. Also $\frac{\chi^2}{\text{d.o.f}} \gg 1$ could be a hint that σ_{cd} is not estimated well. This is why two fits are calculated.
If the three points with $A \in [400, 500]$ are fitted, the result for E_1 is

$$\sigma_{cd} = 0.00216(4) \quad \text{with} \quad \frac{\chi^2}{\text{d.o.f}} = 0.05 \ , \tag{4.4}$$

and for E_3 it is

$$\sigma_{cd} = 0.0024(1) \quad \text{with} \quad \frac{\chi^2}{\text{d.o.f}} = 0.24 \ . \tag{4.5}$$

$\frac{\chi^2}{\text{d.o.f}} \ll 1$ illustrates that it would be possible to put other fits with different σ_{cd} through the three points within the error bars. In contrary if the three points with $A \in [700, 1000]$ are fitted, the result for E_1 is

$$\sigma_{cd} = 0.0015(2) \quad \text{with} \quad \frac{\chi^2}{\text{d.o.f}} = 3.01 \ , \tag{4.6}$$

and for E_3 it is

$$\sigma_{cd} = 0.0016(2) \quad \text{with} \quad \frac{\chi^2}{\text{d.o.f}} = 2.77 \ . \tag{4.7}$$

Here $\frac{\chi^2}{\text{d.o.f}} > 1$ means that it is not possible to fit all three points within the error bars. Probable reasons for this fact are:

- It is possible that the simulation is not exactly performed at the κ-value where $2E_{1,2} = E_3$ is valid.
- For lattices with $A = 27^2, 29^2, 31^2$ $\langle \widetilde{\mathcal{O}_1}^*(0)\widetilde{\mathcal{O}_1}(125)\rangle \sim 10^{-2}$ is an indication that $L_3 = 250$ is not large enough.
- The statistical errors of the energies are possibly underestimated by the procedure described in 3.4.

Chapter 5

Conclusions

5.1 Summary

The estimators of $\langle \widetilde{\mathcal{O}_1}^*(0)\widetilde{\mathcal{O}_1}(x_3 = 0,1)\rangle$ resp. $\langle \mathcal{O}_3(0)\mathcal{O}_3(x_3 = 0,1)\rangle$ with different κ-values have been compared with the analytical calculated $\langle \widetilde{\mathcal{O}_1}^*(0)\widetilde{\mathcal{O}_1}(x_3 = 0,1)\rangle$ resp. $\langle \mathcal{O}_3(0)\mathcal{O}_3(x_3 = 0,1)\rangle$ on a 2^3 lattice in order to make sure that the simulation works well.
Then the improved estimator of $\langle \widetilde{\mathcal{O}_1}^*(0)\widetilde{\mathcal{O}_1}(x_3)\rangle$ is compared with the unimproved one. The difference between the improved and the unimproved estimator is marginal.
The plot of the estimator $\langle \widetilde{\mathcal{O}_1}^*(0)\widetilde{\mathcal{O}_1}(0)\rangle$ for different κ values and different A in figure 4.7 shows, that on a lattice with small A the phase transition occurs within a pseudo-critical region of the κ-value. This leads to the assumption that σ_{cd} is only estimated well using lattices with large A.
The disordered phase of the three-dimensional 3-state Potts model is analogous to the confined phase of the Yang-Mills theory. The three ordered phases correspond to the three deconfined phases. Therefore the three-dimensional 3-state Potts model is an effective theory for the non-zero SU(3) Yang-Mills theory, as K. Holland explains in chapter 4 in [3]. So the calculations in this thesis could be done analogously in the SU(3) Yang-Mills theory.

5.2 Comparison of the obtained σ_{cd} with results from the literature

In [2] the value $\sigma_{cd} = 0.0017(3)$ has been calculated. K. Holland obtained the value $\sigma_{cd} = 0.0015(2)$ in [3]. Only the results in eq.(4.6), (4.7) are in agreement with the measurements of K. Holland and [2]. This confirms the assumption that σ_{cd} is only estimated well using lattices with large A.

5.3 Improvements

A problem during this work was the evaluation of data. In order to calculate the energies from the Monte Carlo measurements a program was written. This took quite a lot of time. The program makes good fits but does not always run smoothly. Especially the estimates of the uncertainties have to be treated with caution. So it would be an improvement to work with an analysis program as for example gnuplot.

In order to confirm that $\sigma_{cd} = 0.0015(2)$ resp. $\sigma_{cd} = 0.0016(2)$, simulations on lattices with $A > 31^2$ and $L_3 > 250$ should be performed. This because with $A > 31^2$ the pseudo-critical region where the phase transition occurs (κ-interval) becomes point like. And if L_3 is large enough $\langle \widetilde{\mathcal{O}_1}^*(0)\widetilde{\mathcal{O}_1}(L_3/2)\rangle \approx 0$.

Chapter 6

Acknowledgements

At this place I want to thank Prof. Uwe-Jens Wiese for giving me the opportunity to write this thesis and for all his help and patience with my questions and programming problems. Many thanks also to Erik Nygren, the discussions with you were very fruitful.

Appendix A

Correlation functions analytically

Here

$$
\begin{aligned}
\langle \widetilde{\mathcal{O}_1}^*(0)\widetilde{\mathcal{O}_1}(x_3)\rangle &= \langle \mathcal{O}_1(0)\mathcal{O}_1(x_3)\rangle + \langle \mathcal{O}_2(0)\mathcal{O}_2(x_3)\rangle \quad \text{with} \\
\langle \mathcal{O}_1(0)\mathcal{O}_1(x_3)\rangle &= \left[\frac{1}{L_1 L_2}\right]^2 \sum_{x_1,x_2,x_1',x_2'} \langle \phi^r(x_1,x_2,0)\phi^r(x_1',x_2',x_3)\rangle \ , \\
\langle \mathcal{O}_2(0)\mathcal{O}_2(x_3)\rangle &= \left[\frac{1}{L_1 L_2}\right]^2 \sum_{x_1,x_2,x_1',x_2'} \langle \phi^i(x_1,x_2,0)\phi^i(x_1',x_2',x_3)\rangle
\end{aligned} \tag{A.1}
$$

and $1 \leq i \leq 3$ and $\phi_x = \phi^r(x_1,x_2,x_3) + i\phi^i(x_1,x_2,x_3)$ are used. $\langle \mathcal{O}_1(0)\mathcal{O}_1(x_3)\rangle$ and $\langle \mathcal{O}_2(0)\mathcal{O}_2(x_3)\rangle$ are both not invariant under rotations (see section 2.2). But the combination of both $\langle \widetilde{\mathcal{O}_1}^*(0)\widetilde{\mathcal{O}_1}(x_3)\rangle$ is invariant under rotations. The following calculation is similar to the calculation done in [2].

It is possible to link the energy eigenstates in the spectrum of the transfer matrix in the x_3-direction with the measured operators in section 3.3.

$$
\begin{aligned}
\mathcal{Z}\langle \mathcal{O}_i(0)\mathcal{O}_i(x_3)\rangle &= \sum_n \langle n \mid \mathcal{O}_i \mathrm{e}^{-\mathcal{H}x_3}\mathcal{O}_i \mathrm{e}^{-\mathcal{H}(L_3-x_3)} \mid n\rangle \\
&= \sum_{m,n} \langle n \mid \mathcal{O}_i \mid m\rangle \mathrm{e}^{-E_m x_3} \langle m \mid \mathcal{O}_i \mid n\rangle \mathrm{e}^{-E_n(L_3-x_3)} \\
&= \sum_{m,n} \mid \langle n \mid \mathcal{O}_i \mid m\rangle \mid^2 \mathrm{e}^{-E_m x_3}\mathrm{e}^{-E_n(L_3-x_3)} \quad \text{where} \\
\mathcal{Z} &= \sum_n \langle n \mid \mathrm{e}^{-\mathcal{H}L_3} \mid n\rangle = \sum_n \mathrm{e}^{-E_n L_3} \\
&\approx 1 + \mathrm{e}^{-E_1 L_3} + \mathrm{e}^{-E_2 L_3} + \mathrm{e}^{-E_3 L_3} \ .
\end{aligned} \tag{A.2}
$$

Then some straightforward calculations lead to the following expression

$$\begin{aligned}
\mathcal{Z}\langle\mathcal{O}_i(0)\mathcal{O}_i(x_3)\rangle \approx & \mid\langle 0\mid\mathcal{O}_i\mid 0\rangle\mid^2+\mid\langle 1\mid\mathcal{O}_i\mid 0\rangle\mid^2\left[\mathrm{e}^{-E_1(L_3-x_3)}+\mathrm{e}^{-E_1x_3}\right] \\
& +\mid\langle 2\mid\mathcal{O}_i\mid 0\rangle\mid^2\left[\mathrm{e}^{-E_2(L_3-x_3)}+\mathrm{e}^{-E_2x_3}\right] \\
& +\mid\langle 3\mid\mathcal{O}_i\mid 0\rangle\mid^2\left[\mathrm{e}^{-E_3(L_3-x_3)}+\mathrm{e}^{-E_3x_3}\right] \\
& +\mid\langle 1\mid\mathcal{O}_i\mid 1\rangle\mid^2\mathrm{e}^{-E_1L_3}+\mid\langle 2\mid\mathcal{O}_i\mid 2\rangle\mid^2\mathrm{e}^{-E_2L_3} \\
& +\mid\langle 3\mid\mathcal{O}_i\mid 3\rangle\mid^2\mathrm{e}^{-E_3L_3} \\
& +\mid\langle 1\mid\mathcal{O}_i\mid 2\rangle\mid^2\left[\mathrm{e}^{-E_1(L_3-x_3)-E_2x_3}+\mathrm{e}^{-E_1x_3-E_2(L_3-x_3)}\right] \\
& +\mid\langle 1\mid\mathcal{O}_i\mid 3\rangle\mid^2\left[\mathrm{e}^{-E_1(L_3-x_3)-E_3x_3}+\mathrm{e}^{-E_1x_3-E_3(L_3-x_3)}\right] \\
& +\mid\langle 2\mid\mathcal{O}_i\mid 3\rangle\mid^2\left[\mathrm{e}^{-E_2(L_3-x_3)-E_3x_3}+\mathrm{e}^{-E_2x_3-E_3(L_3-x_3)}\right] \ . \qquad \text{(A.3)}
\end{aligned}$$

Terms with energies larger than E_3 and terms including 2nth ore higher powers of energies are neglected. The operator $\mathcal{O}_1$ is symmetric under charge conjugation and belongs to the mixed irreducible representation of S_3. The operator $\mathcal{O}_2$ is antisymmetric under charge conjugation and belongs to the mixed irreducible representation of S_3. The operator $\mathcal{O}_3$ is invariant under charge conjugation and belongs to the symmetric irreducible representation of S_3. Then $\mid 1\rangle$ is symmetric under charge conjugation and belongs to the mixed irreducible representation of S_3. $\mid 2\rangle$ is antisymmetric under charge conjugation and belongs to the mixed irreducible representation of S_3. $\mid 3\rangle$ and $\mid 0\rangle$ are invariant under charge conjugation and belong to the symmetric irreducible representation of S_3. Moreover the following expressions are used

$$\begin{aligned}
\langle\text{mixed}\mid\text{symmetric}\rangle=0, \qquad & \langle\text{mixed}\mid\text{antisymmetric}\rangle=0, \\
\langle\text{symmetric}\quad\mid\quad\text{antisymmetric}\rangle=0\ . & \qquad \text{(A.4)}
\end{aligned}$$

Because of the S_3 symmetry, the relations

$$E_1=E_2, \quad \mid\langle 1\mid\mathcal{O}_1\mid 0\rangle\mid^2=\mid\langle 2\mid\mathcal{O}_2\mid 0\rangle\mid^2 \quad \text{and} \quad \mid\langle 1\mid\mathcal{O}_1\mid 3\rangle\mid^2=\mid\langle 2\mid\mathcal{O}_2\mid 3\rangle\mid^2 \quad \text{(A.5)}$$

are fulfilled.
This leads to

$$\begin{aligned}
\mathcal{Z}\langle\mathcal{O}_1(0)\mathcal{O}_1(x_3)\rangle &\approx \mid\langle 1\mid\mathcal{O}_1\mid 0\rangle\mid^2\left[\mathrm{e}^{-E_1(L_3-x_3)}+\mathrm{e}^{-E_1x_3}\right] \\
&\quad+\left[\mid\langle 1\mid\mathcal{O}_1\mid 1\rangle\mid^2+\mid\langle 2\mid\mathcal{O}_1\mid 2\rangle\mid^2\right]\mathrm{e}^{-E_1L_3} \\
&\quad+\mid\langle 1\mid\mathcal{O}_1\mid 3\rangle\mid^2\left[\mathrm{e}^{-E_1(L_3-x_3)-E_3x_3}+\mathrm{e}^{-E_1x_3-E_3(L_3-x_3)}\right] \;, \qquad \text{(A.6)} \\
\mathcal{Z}\langle\mathcal{O}_2(0)\mathcal{O}_2(x_3)\rangle &\approx \mid\langle 1\mid\mathcal{O}_1\mid 0\rangle\mid^2\left[\mathrm{e}^{-E_1(L_3-x_3)}+\mathrm{e}^{-E_1x_3}\right] \\
&\quad+2\mid\langle 1\mid\mathcal{O}_2\mid 2\rangle\mid^2\mathrm{e}^{-E_1L_3} \\
&\quad+\mid\langle 1\mid\mathcal{O}_1\mid 3\rangle\mid^2\left[\mathrm{e}^{-E_1(L_3-x_3)-E_3x_3}+\mathrm{e}^{-E_1x_3-E_3(L_3-x_3)}\right] \;, \qquad \text{(A.7)} \\
\mathcal{Z}\langle\mathcal{O}_3(0)\mathcal{O}_3(x_3)\rangle &\approx \mid\langle 0\mid\mathcal{O}_3\mid 0\rangle\mid^2 \\
&\quad+\mid\langle 3\mid\mathcal{O}_3\mid 0\rangle\mid^2\left[\mathrm{e}^{-E_3(L_3-x_3)}+\mathrm{e}^{-E_3x_3}\right] \\
&\quad+\left[\mid\langle 1\mid\mathcal{O}_3\mid 1\rangle\mid^2+\mid\langle 2\mid\mathcal{O}_3\mid 2\rangle\mid^2\right]\mathrm{e}^{-E_1L_3} \\
&\quad+\mid\langle 3\mid\mathcal{O}_3\mid 3\rangle\mid^2\mathrm{e}^{-E_3L_3} \;. \qquad \text{(A.8)}
\end{aligned}$$

The derivation of the improved estimator in section 3.3 shows, that the estimators of $\langle\mathcal{O}_1(0)\mathcal{O}_1(x_3)\rangle$ and $\langle\mathcal{O}_2(0)\mathcal{O}_2(x_3)\rangle$ have to be equal.
Therefore $\mid\langle 1\mid\mathcal{O}_1\mid 1\rangle\mid^2+\mid\langle 2\mid\mathcal{O}_1\mid 2\rangle\mid^2=2\mid\langle 1\mid\mathcal{O}_2\mid 2\rangle\mid^2$ is assumed.
Then at large x_3 the correlation functions take the form

$$\begin{aligned}
\langle\widetilde{\mathcal{O}_1}^*(0)\widetilde{\mathcal{O}_1}(z)\rangle &\approx A+B\cosh\left[E_1\left(\frac{L_3}{2}-x_3\right)\right] \;, \\
\langle\mathcal{O}_3(0)\mathcal{O}_3(x_3)\rangle &\approx C+D\cosh\left[E_3\left(\frac{L_3}{2}-x_3\right)\right] \;. \qquad \text{(A.9)}
\end{aligned}$$

A, B, C, D are constants which depend on L_3.

Appendix B

The trace of transfer matrix products

A transfer matrix which describes the microscopical evolution of the spin configuration from one x-y-plane l to the neighboring x-y-plane m is defined as

$$\langle \phi^l \mid T \mid \phi^m \rangle = \mathrm{e}^{\frac{\kappa}{2}\sum_{\langle xy\rangle}\delta_{\phi_x^l,\phi_y^l}}\mathrm{e}^{\frac{\kappa}{2}\sum_{\langle xy\rangle}\delta_{\phi_x^m,\phi_y^m}}\mathrm{e}^{\kappa\sum_{\langle xy\rangle}\delta_{\phi_x^l,\phi_y^m}} \ , \tag{B.1}$$

as it is written in section 2.5. Then

$$\begin{aligned}
\mathrm{Tr}[T^{L_3}] &= \sum_l \langle \phi^l \mid T^{L_3} \mid \phi^l \rangle = \sum_{l,k_1,..,k_{L_3-1}} \langle \phi^l \mid T \mid \phi^{k_1}\rangle\langle \phi^{k_1} \mid T \mid \phi^{k_2}\rangle \cdots \langle \phi^{k_{L_3-1}} \mid T \mid \phi^l \rangle \\
&= \sum_{l,k_1,..,k_{L_3-1}} \exp\left[\frac{\kappa}{2}\sum_{\langle xy\rangle}\delta_{\left(\phi_x^l,\phi_y^l\right)} + \frac{\kappa}{2}\sum_{\langle xy\rangle}\delta_{\left(\phi_x^{k_1},\phi_y^{k_1}\right)} + \kappa\sum_{\langle xy\rangle}\delta_{\left(\phi_x^l,\phi_y^{k_1}\right)}\right] \\
&\exp\left[\frac{\kappa}{2}\sum_{\langle xy\rangle}\delta_{\left(\phi_x^{k_1},\phi_y^{k_1}\right)} + \frac{\kappa}{2}\sum_{\langle xy\rangle}\delta_{\left(\phi_x^{k_2},\phi_y^{k_2}\right)} + \kappa\sum_{\langle xy\rangle}\delta_{\left(\phi_x^{k_1},\phi_y^{k_2}\right)}\right]\cdots \\
&\cdots\exp\left[\frac{\kappa}{2}\sum_{\langle xy\rangle}\delta_{\left(\phi_x^{k_{L_3-1}},\phi_y^{k_{L_3-1}}\right)} + \frac{\kappa}{2}\sum_{\langle xy\rangle}\delta_{\left(\phi_x^l,\phi_y^l\right)} + \kappa\sum_{\langle xy\rangle}\delta_{\left(\phi_x^{k_{L_3-1}},\phi_y^l\right)}\right] \\
&= \sum_{l,k_1,..,k_{L_3-1}} \exp\left[\kappa\left(\sum_{\langle xy\rangle}\delta_{\left(\phi_x^l,\phi_y^l\right)} + \sum_{\langle xy\rangle}\delta_{\left(\phi_x^{k_1},\phi_y^{k_1}\right)} + \sum_{\langle xy\rangle}\delta_{\left(\phi_x^{k_2},\phi_y^{k_2}\right)} + \cdots + \sum_{\langle xy\rangle}\delta_{\left(\phi_x^{k_{L_3-1}},\phi_y^{k_{L_3-1}}\right)}\right)\right] \\
&\exp\left[\kappa\left(\sum_{\langle xy\rangle}\delta_{\left(\phi_x^l,\phi_y^{k_1}\right)} + \sum_{\langle xy\rangle}\delta_{\left(\phi_x^{k_1},\phi_y^{k_2}\right)} + \cdots + \sum_{\langle xy\rangle}\delta_{\left(\phi_x^{k_{L_3-1}},\phi_y^l\right)}\right)\right] \\
&= \left[\prod_{x'}\sum_{\phi_{x'}\in\mathbb{Z}(3)}\right] \mathrm{e}^{\kappa\sum_{\langle xy\rangle}\delta_{\phi_x,\phi_y}} = \mathcal{Z} \ ,
\end{aligned} \tag{B.2}$$

as it is expected for a transfer matrix.

Bibliography

[1] B. A. Berg. Introduction to Markov Chain Monte Carlo Simulations and their Statistical Analysis. http://adsabs.harvard.edu/abs/2004cond.mat.10490B, October 2004.

[2] B. Grossmann, M.L. Laursen, T. Trappenberg, and U.J. Wiese. The confined - deconfined interface tension and the spectrum of the transfer matrix. Nucl.Phys., B396:584-610, 1993.

[3] K. Holland. Confinement and deconfinement in gauge theories. PhD thesis, Massachusetts Institute of Technology, 1999.

[4] W. Janke and R. Villanova. Three-dimensional three state Potts model revisited with new techniques. Nucl.Phys., B489:679-696, 1997.

[5] R. Lipowsky. Critical behavior of interfaces: Wetting, surface melting and related phenomena. Zentralbibliothek d. Kernforschungsanlage, 1987.

[6] Erik Nygren. Monte Carlo study of interface dynamics in the 3-d 3-state Potts model. Master thesis, University of Bern, 2012.

[7] R. H. Swendsen and J.-S. Wang. Nonuniversal critical dynamics in Monte Carlo simulations. Phys. Rev. Lett., 58:86-88, Jan 1987.

[8] U.J. Wiese. Sign and Complex Action Problems: The Potts Model Approximation to Dense QCD as a Solvable Example. http://www.wiese.itp.unibe.ch/lectures.html, May 2006.

[9] U.J. Wiese. An Introduction to Lattice Field Theory. http://www.wiese.itp.unibe.ch/lectures.html, August 2009.

[10] F. Y. Wu. The Potts model. Rev. Mod. Phys., 54:235-268, http://link.aps.org/doi/10.1103/RevModPhys.54.235, Jan 1982.

[11] P. Young. Jackknife and Bootstrap Resampling Methods in Statistical Analysis to Correct for Bias. Physics Departement, University of California Santa Cruz, Santa Cruz CA 95064, http://maxwell.ucsc.edu/~peter/jackboot.pdf.